RESEARCH ON FLOW CHANNEL STRUCTURE OPTIMIZATION OF CYCLOPENTANE REGENERATOR PRINTED CIRCUIT HEAT EXCHANGER

Mengdi SONG[1], Hongfei ZHANG[1,*], Xun WANG[2], Junhao YANG[1], Cheng WANG[1],

Yuanxun DING[2]

[*1]The College of Advanced Manufacturing Engineering, Hefei University, Hefei 230601, China.

[2]State Key Laboratory of Engines, Tianjin University, 92 Weijin Road, Nankai District, Tianjin 300072, China

[*]Corresponding author; E-mail: zhanghf@ hfuu.edu.cn

To enhance the cyclopentane regenerator performance of the Organic Rankine Cycle system, this study optimizes the flow channel structure of the printed circuit heat exchanger via CFD multi-physics coupling simulation. Three-dimensional models of straight-flow, reflux-flow, and cross-flow channels are established, and their thermo-hydraulic performances are systematically compared. Results show that the cross-flow channel achieves the best overall performance, with a cold-side pressure drop of 0.65 kPa, hot-side pressure drop of 0.24 kPa, and heat-transfer rate of 2.39 kW. The heat-transfer rate is 198.75% higher than the straight-flow channel, while the cold and hot-side pressure drops are reduced by 60.61% and 87.88% compared with the reflux-flow channel. Heat-transfer correlations for hot and cold sides are fitted using multi-condition data and genetic algorithm. Experimental verification shows errors within 15% for the hot side and 18% for the cold side, providing a high-precision theoretical model for Printed Circuit Heat Exchanger engineering design in Organic Rankine Cycle systems.

Keywords*: Cyclopentane; Organic Rankine Cycle; Printed Circuit Heat Exchanger; CFD Fluent simulation*

1.Introduction

Owing to factors like low global energy utilization efficiency, excessive resource consumption, and growing environmental awareness, efficient energy utilization has emerged as a key challenge for modern society[1]. In current industrial processes, a significant amount of energy is lost in the form of waste heat[2]. This is particularly evident in high-temperature heat sources such as gas turbines, where the utilization rate of waste heat is relatively low[3]. Data show that about 50% of industrial energy is wasted as thermal energy, mainly from high-temperature equipment such as gas turbines and internal combustion engines[4, 5]. Thermal energy recovery from industrial and mechanical equipment has become an effective way to improve energy efficiency and reduce energy consumption[6].

Converting heat from low-temperature heat sources into usable energy is the core challenge of waste - heat recovery. Traditional waste heat recovery technologies often fail to meet performance expectations in low-temperature scenarios[7]. Compared with Organic Rankine Cycle (ORC),

Supercritical Rankine Cycle (SRC), and Supercritical Brayton Cycle (SBC), ORC is most suitable for low-temperature waste heat recovery[8]. Dong et al. proposed a graphical method for integrating waste heat streams with ORC systems to clearly demonstrate flow characteristics and parameter selection[9]. Combining three-stage expansion with an ejector cycle can achieve deep recovery of engine waste heat[10]. ORC can improve energy efficiency and reduce emissions, and optimizing ORC configurations can determine the optimal heat exchange structure[11-14].

Cyclopentane is an environmentally friendly refrigerant, which is characterized by its low toxicity, low ODP value, and high thermal stability, making it suitable for refrigeration and heat pump applications. Its low boiling point of 49 ℃, relatively high thermal efficiency, and low GWP render it an ideal working fluid for waste heat recovery[15]. Pentane, an alkane working fluid, shows excellent thermodynamic performance in high-temperature waste-heat recovery within the ORC system. The ORC plays a key role in waste-heat recovery and power generation from low-temperature heat sources. Testing various working fluids confirms that the ORC delivers outstanding performance in clean-energy recovery[16]. However, targeted studies on cyclopentane–Printed Circuit Heat Exchanger (PCHE) coupling in ORC regenerators remain insufficient, and reliable design guidelines are still lacking[17].

PCHE is widely recognized in ORC systems and low-temperature waste heat recovery, effectively enhancing secondary energy utilization and industrial energy conservation[18, 19]. As waste heat recovery technology advances, PCHE is being applied to ORC systems due to its large heat transfer area, excellent performance, and high pressure resistance[20, 21]. Its micro channel structure can increase surface area, while its compact design makes it well-suited for industrial waste heat recovery scenarios[22].Recent studies have also confirmed the advantages of PCHE in thermal–hydraulic performance and structural optimization for advanced heat recovery systems[23].

PCHE improves heat transfer and reduces size, offering new insights for refrigeration heat exchanger design. Its advanced use achieves high energy efficiency without excessive volume, cutting costs and footprint. However, PCHEs still have limitations requiring further improvement in application and design[24, 25]. Uneven flow distribution, high flow resistance, and micro channel heat transfer efficiency are all issues that still need to be addressed in the future. The thermal and flow characteristics in microchannels are significantly influenced by channel structure and flow pattern, which determine the overall heat transfer performance and flow resistance of heat exchangers[26]. Micro - channel geometry can be modified to study heat - transfer performance. Xin et al. found that different PCHE micro channel designs affect heat - transfer efficiency and pressure drop. Optimizing micro channel design improves PCHE heat transfer efficiency and ORC system performance[27].

The relatively high viscosity and low thermal conductivity of cyclopentane make the PCHE more complex. The Fluent module is used to simulate the flow and heat transfer of the fluid inside the heat exchanger, which helps to calculate the flow - field distribution, heat transfer efficiency, and flow resistance[28]. The dimensions of the rectangular micro channels have an impact on their heat transfer and flow - performance characteristics, with the cross - sectional area and height of the channels being decisive factors[29].

Current studies lack in-depth investigations on cyclopentane-microchannel coupling, especially systematic engineering analysis. Therefore, this study establishes three microchannel models to explore cyclopentane heat transfer and flow characteristics via CFD, visualizes thermal and pressure fields, and develops high-precision heat transfer correlations. It aims to fill the research gap in the collaborative

optimization of cyclopentane and complex microchannels, reveal the geometric coupling mechanism affecting flow resistance and heat transfer of high-viscosity fluids, and build a reliable performance prediction model.

2. Theory and Methodology

2.1. The physical properties of pentane

The thermodynamic properties of pentane are decisive for the efficiency and operating performance of heat exchangers, and the relevant patterns have been elaborated in previous studies[30]：Gaseous and liquid pentane exhibit significant physical property differences with temperature, as shown in prior studies. At 290 K, their densities are about 2.5 kg/m³ (gas) and 740 kg/m³ (liquid). Liquid pentane has much higher viscosity than the gas, increasing flow resistance and pumping power in heat exchangers. The gas, with low density and viscosity, offers better fluidity and more efficient heat transfer.

2.2. The Structure of the Printed-Circuit Heat Exchanger

Fig. 1(a) shows a prototype of the straight-channel recuperator (PCHE), where red arrows indicate the flow direction of gaseous cyclopentane and blue arrows indicate that of liquid cyclopentane; Fig. 1(b) is a schematic diagram of its model. The printed circuit heat exchanger is assembled from thin metal sheets fabricated by an embossing process and arranged in a regular pattern, fabricated with stainless steel. Its heat transfer plates are flat, with surfaces specially treated to form corrugations or fins, which effectively enhance heat transfer performance by increasing the heat transfer area and promoting fluid turbulence.

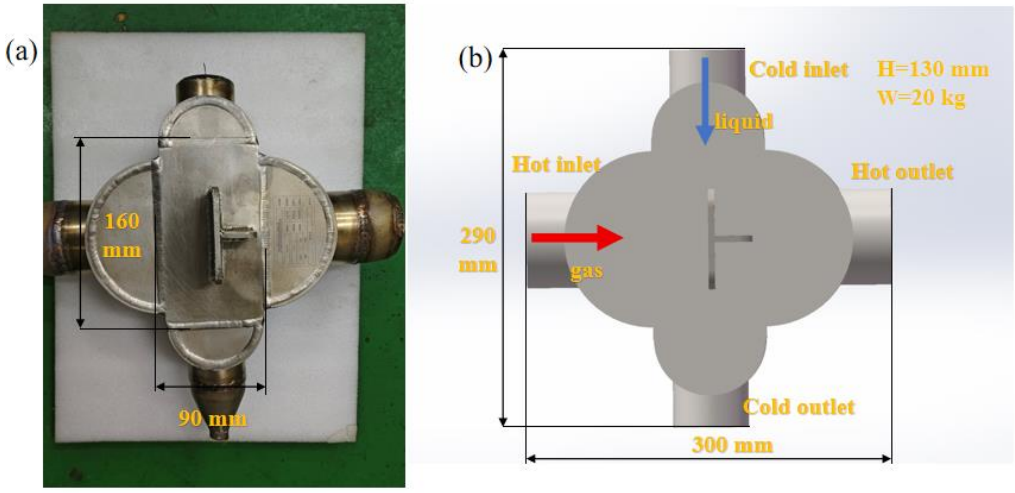

Figure 1. Schematic diagram of PCHE structure (a) Physical picture (b) Model picture

Tab. 1 presents the basic specifications of the PCHE, with core dimensions of 160 mm (L) × 90 mm (W) × 130 mm (H). It is a compact heat exchanger that is convenient for installation and use in engineering applications. Generally, thinner plates are preferable—provided adequate strength and rigidity are maintained. The channels between plates are formed by stacking and compression, creating long, narrow, and tortuous passages to ensure sufficient heat transfer area for both hot and cold fluids.

The structural parameters and dimensions of the PCHE core, including length, width, height, heat transfer area, channel hole count, and plate number, are determined based on typical design criteria and engineering practices of compact printed circuit heat exchangers for ORC waste heat recovery systems. The geometric configuration and channel layout meet the requirements of structural strength, heat transfer performance, and chemical etching machinability.

Table 1. Basic parameters of the tested PCHE

Parameter [Unit]	Values
Length of core size [mm]	160
Width of core size [mm]	90
Height of core size [mm]	130
Heat-transfer area (hot side) [m^2]	0.72
Heat-transfer area (cold side) [m^2]	1.4
Number of channel holes (hot side) [-]	49
Number of channel holes (cold side) [-]	9
Number of plates (hot side) [-]	40
Number of plates (cold side) [-]	40

2.3. Comparison of Three Flow-Channel Structures

This study proposes three flow channel structures for cyclopentane heat transfer performance in printed circuit heat exchangers. As shown in Fig. 2(a), the straight-channel design offers a simple layout with fast fluid flow and low resistance, suitable for pressure-drop-sensitive applications requiring high flow efficiency, but it is prone to local heat transfer non-uniformity. It should be clarified that the straight channel has the shortest flow path and weakest turbulence, thus presenting the lowest heat transfer performance. Fig. 2 (b) shows that the return-flow channel enhances heat transfer by extending flow path length and contact area through folded passages, enabling it to handle high heat loads, though at the cost of significantly increased flow resistance. The zigzag channel in Fig. 2(c) achieves a balance between low resistance and strong heat transfer by disturbing the fluid through tortuous paths, with its resistance and heat transfer performance lying between the two aforementioned designs.

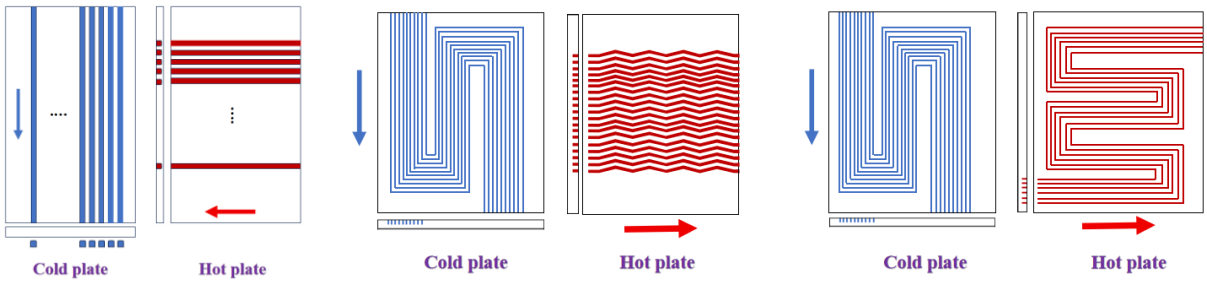

(a) (b) (c)

Figure 2. Three types of flow channel structures：(a) Straight-Flow Channel; (b) Reflux Flow Channel; (c) Zigzag Flow Channel

2.4. Simulation Method

Computational Fluid Dynamics (CFD) is used to study the flow and heat - transfer characteristics of fluids (such as cyclopentane). When simulating a cyclopentane printed-circuit regenerator, CFD can provide detailed data on velocity, pressure, temperature, etc. The general process includes: simplifying the geometric model, meshing (which affects accuracy and speed), setting boundary conditions (such as inlet and outlet parameters), and choosing an appropriate turbulence model (which is crucial for the results). These steps ensure that the simulation results are accurate and reliable.

The equations used in the simulation are as follows[31]:

Continuity Equation:

$$\frac{\partial}{\partial x_i}(\rho u_i) = 0 \tag{1}$$

Momentum Equation:

$$\frac{\partial}{\partial x_i}(\rho u_i u_j) = -\frac{\partial P}{\partial x_i} + \rho g_i + \frac{\partial}{\partial x_i}\left[(\mu_t + \mu_s)\frac{\partial \mu_i}{\partial x_i}\right] \tag{2}$$

Energy Equation:

$$\frac{\partial}{\partial x_i}\left(u_i(\rho E + p)\right) = \frac{\partial}{\partial x_i}\left(k_{eff}\frac{\partial T}{\partial x_i} + u_i T_{ij}\right) \tag{3}$$

In these equations, u_i represents the velocity vector, P is the pressure, u_t and u_s are the turbulent viscosity and molecular viscosity respectively, k_{eff} denotes the effective thermal conductivity, and λ is the turbulent thermal conductivity. In this study, the SST κ-ω model is selected for turbulence simulation, and the second-order upwind scheme is used for calculation. Meanwhile, the convergence criterion of the residual convergence method is set to 10^{-6} to ensure the accuracy of the simulation results.

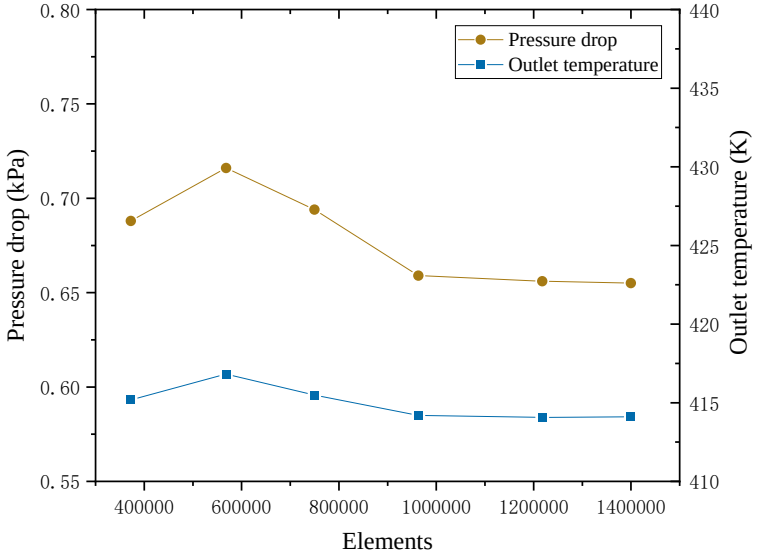

Figure 3. Grid independence verification

Grid independence. Owing to the complex flow channel structure of PCHE, ANSYS meshing was employed to generate unstructured grids with refined wall and corner regions. To ensure numerical

accuracy and efficiency, a grid independence study was conducted using six grid densities: 372489, 568134, 749671, 963205, 1217842 and 1400000 elements, as shown in Fig. 3. The results confirm grid independence. Considering accuracy and efficiency, the grid with 963205 elements was adopted for all simulations.

The boundary conditions including inlet temperature, mass flow rate and operating pressure are set according to the typical operating ranges of cyclopentane-based organic Rankine cycle regenerators reported in published studies and engineering applications. Such settings ensure that the simulation conditions are representative and consistent with actual working conditions.

The detailed boundary conditions of the CFD model are defined as follows. The hot and cold fluid inlets are both set as mass flow inlets with specified mass flow rate and inlet temperature. The outlets are defined as pressure outlets with fixed back pressure. All solid wall surfaces adopt no-slip boundary condition, and the walls are set as adiabatic with zero heat flux to eliminate external heat loss. The hot fluid inlet pressure is 1000 kPa, and the cold fluid inlet pressure is 150 kPa. The mass flow rate ranges from 0.0036 kg/s to 0.1215 kg/s, which is consistent with the actual operating parameters of ORC regenerators.

A comparison of various turbulence models demonstrates that the SST κ-ω model is optimal for PCHE microchannels. As presented in Fig. 5, the deviations between simulation and experiment are within 6% for both outlet temperature and pressure drop, verifying the reliability and accuracy of the selected model[30]. Model validation is crucial for the accuracy of simulation experiments. By comparing the simulated data with experimental data on outlet temperature and pressure drop, as shown in Fig. 4, the error in outlet temperature ranges from 1% to 4%, with the maximum being 3.1%. The error in pressure drop is around 5%, with the maximum error being 5.5%. These data effectively validate the accuracy of the simulation.

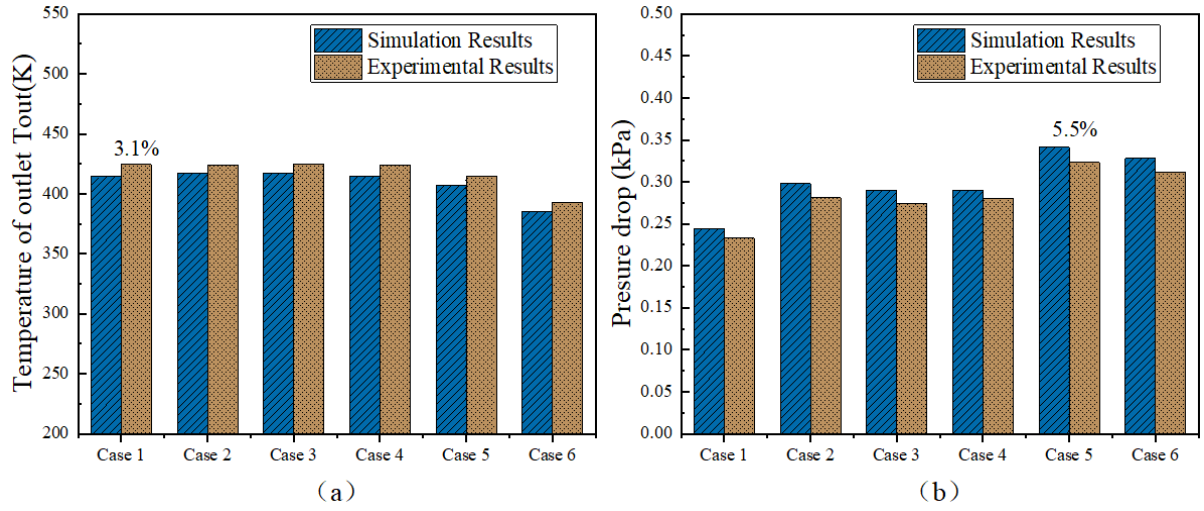

Figure 4. Comparison of Experimental and Simulation Results: (a) Heat Transfer Performance; (b) Pressure - Drop Performance

3. Simulation Results and Analysis

3.1. Temperature and Pressure Analysis of the Straight-Flow Structure

The simulation results clearly illustrate the temperature and pressure conditions of the PCHE structure. In Fig. 5(a), the cold fluid flows from left to right, with a significant temperature difference in the channel. The upper area near the hot fluid inlet is hotter, while the lower area is colder. Due to continuous heat absorption, the cold fluid's temperature gradually rises and eventually reaches thermal equilibrium. In Fig. 5(b), the hot fluid flows from top to bottom, showing a similar temperature gradient. This structure effectively avoids local overheating or overcooling, ensuring stable operation.

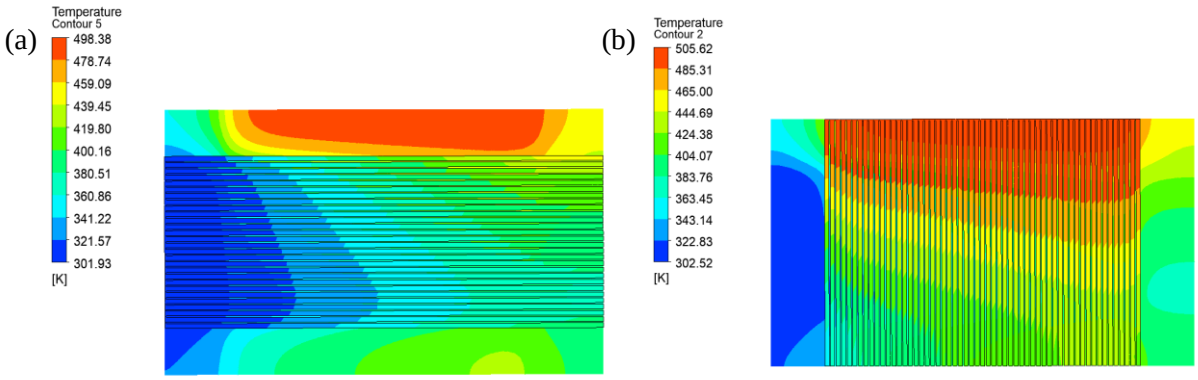

Figure 5. Temperature Distribution Contour: (a) Cold Fluid; (b) Hot Fluid

The pressure distribution in Fig. 6 shows that pressure decreases along the flow direction, consistent with the fundamental principles of fluid mechanics. The cold fluid exhibits more significant pressure variation because its rising temperature reduces viscosity and density, decreasing flow resistance and resulting in more pronounced pressure changes. The hot fluid shows relatively smaller pressure variation, as its physical properties remain relatively stable under experimental conditions, with pressure loss controlled within a reasonable range.

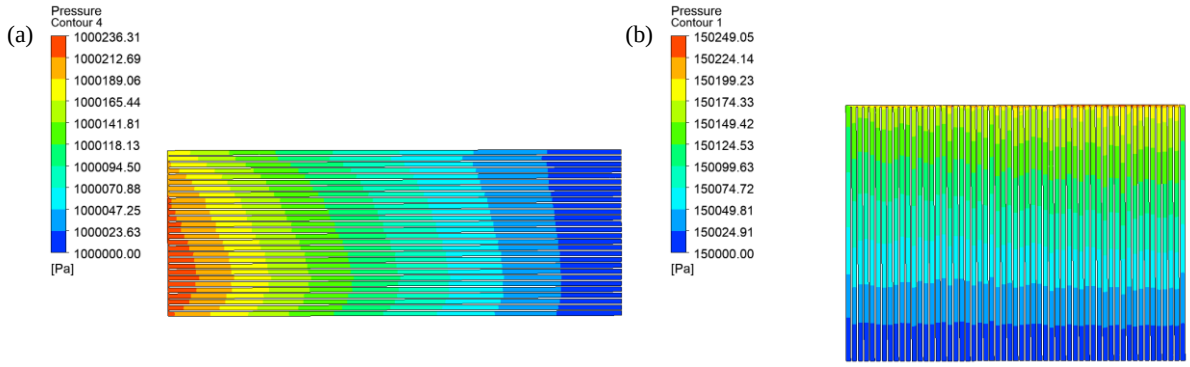

Figure 6. Pressure Distribution Contour: (a) Cold Fluid; (b) Hot Fluid

The temperature distribution shows a gradual and stable variation along the flow path, which is caused by the steady flow and weak disturbance in the straight channel. The thermal boundary layer fully develops along the smooth channel and becomes thicker, thus reducing the heat transfer intensity.

The pressure loss mainly originates from the wall friction along the flow path, and no obvious local pressure loss is observed at bending or turning positions.

3.2. Temperature and Pressure Analysis of the Reflux Structure

Fig. 7(a) shows cold fluid flowing left to right, with a left-low, right-high temperature gradient. The serpentine channel extends heat transfer. Fig. 7(b) has hot fluid flowing top to bottom, with a bottom-low, top-high gradient and uniform upper temperature, enhancing heat transfer efficiency.

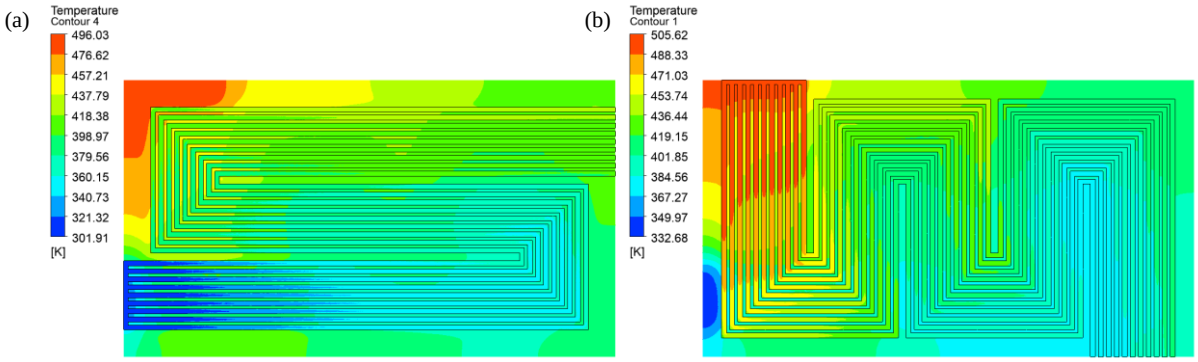

Figure 7. Temperature Distribution Contour: (a) Cold Fluid; (b) Hot Fluid

Fig. 8(a) shows the cold fluid pressure varies smoothly with the flow path, following fluid dynamics principles. Its pressure drop is temperature-dependent: higher temperatures reduce flow resistance and pressure loss, confirming that friction causes pressure loss and regular channel structures control pressure gradients. Fig. 8(b) shows the hot fluid pressure decreases along the path, with an inlet-outlet difference of~20.7 kPa. Pressure changes are most significant at bends, reflecting high flow resistance and a distinct pressure gradient. This provides insights for understanding fluid pressure variations and optimizing channel design.

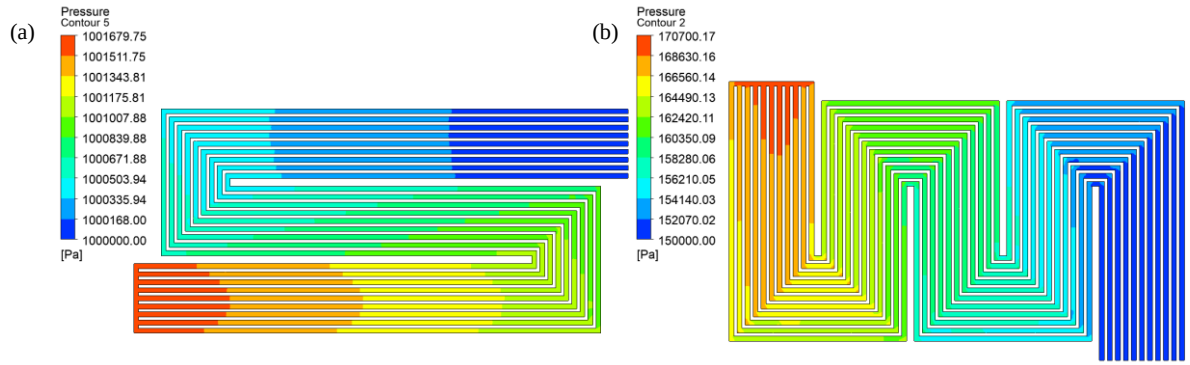

Figure 8. Pressure Distribution Contour: (a) Cold Fluid; (b) Hot Fluid

The reflux channel extends the flow path and forms local flow recirculation, which prolongs the fluid residence time and improves heat transfer uniformity. However, flow separation and vortices at the turning points lead to obvious local pressure loss, resulting in a significant increase in overall flow resistance.

3.3. Temperature and Pressure Analysis of the Zigzag Structure

Fig. 9 presents the temperature and pressure fields of the recuperator. The zigzag structure enhances heat transfer and turbulence, with a temperature range of 301.9–473.2 K. The serpentine channel prolongs residence time, achieving a temperature range of 305.8–505.6 K and more sufficient heat exchange. Performance differences between the two structures provide a key basis for structural selection and thermal design optimization.

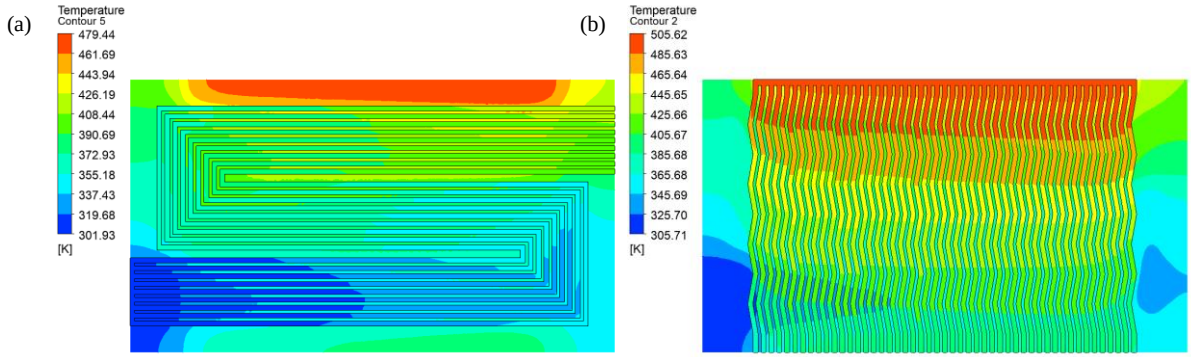

Figure 9. Temperature Distribution Contour: (a) Cold Fluid; (b) Hot Fluid

Fig. 10 presents pressure distributions of two channels. The serpentine channel shows obvious pressure changes at bends, with pressure drops of 1.5 kPa and 0.3 kPa. The wave-shaped channel presents a gradient distribution. Different structures lead to different flow resistances, providing a reference for structural optimization to reduce energy loss.

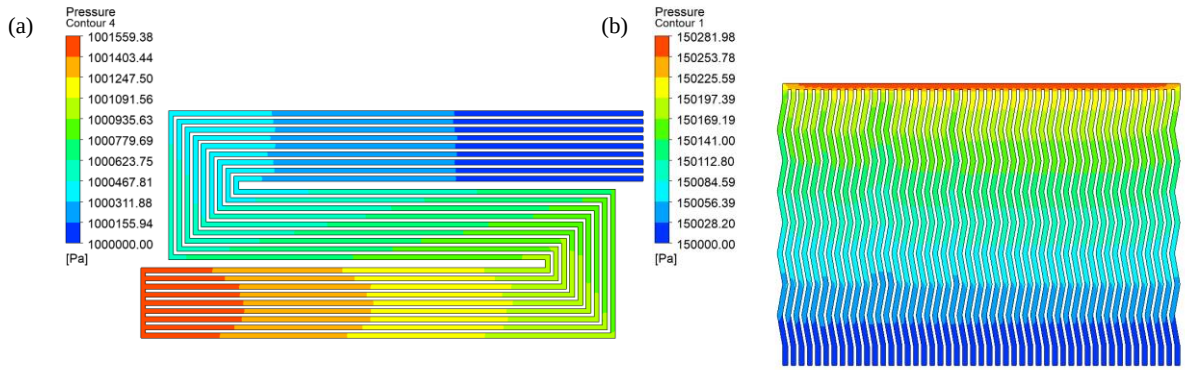

Figure 10. Pressure Distribution Contour: (a) Cold Fluid; (b) Hot Fluid

The tortuous flow path repeatedly disrupts the development of the thermal boundary layer and enhances fluid mixing. The bending sections promote flow disturbance and improve the heat transfer effect. The pressure variation is concentrated at the bending positions, which reflects the influence of flow direction change on the pressure distribution.

3.4. Comparison of the Performance of the Three Flow Channels

The three flow channels have different structural configurations, leading to differences in flow path length and heat transfer area. The comparison is carried out under the same core volume and boundary conditions. Fig. 11 compares the pressure drops on the cold and hot sides and the heat transfer rate for

three channel types: straight-flow, return-flow, and zigzag-flow. The straight-flow channel has the shortest flow path and weak turbulence, resulting in the lowest heat transfer rate. The zigzag-flow channel delivers significant advantages: 60.61% lower cold-side pressure drop (0.65 kPa vs 1.65 kPa) and 87.88% lower hot-side drop (0.24 kPa vs 1.98 kPa) than the return-flow channel, cutting pumping energy use. Its 2.39 kW heat transfer rate is 57.24% higher than the return-flow channel and 198.75% higher than the straight-flow channel (0.8 kW). Balancing high efficiency and low pressure drop, it outperforms both other channels and suits pressure-drop-sensitive applications.

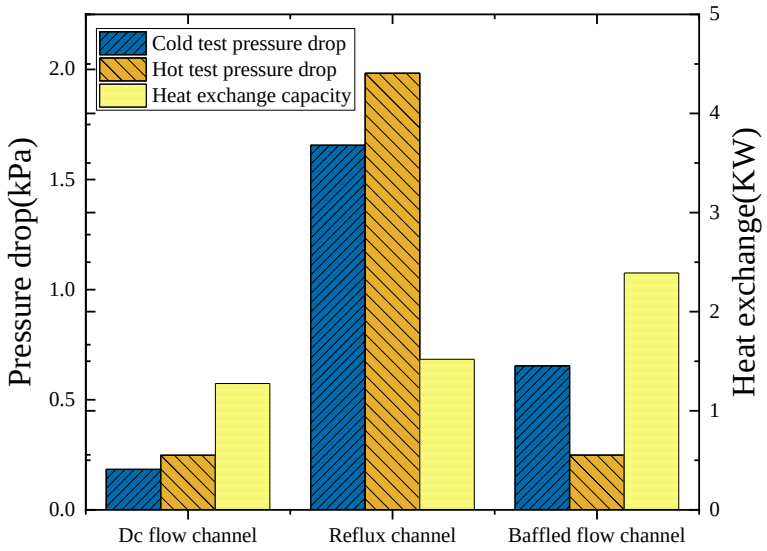

Figure 11. Comparison of Different Flow-Channel Characteristics

To further analyze the energy utilization efficiency and irreversible loss, entropy generation analysis is carried out according to the methods in Refs[32, 33].

The total entropy generation consists of heat transfer entropy generation and viscous dissipation entropy generation:

$$S_{total} = S_h + S_d \tag{4}$$

The heat transfer entropy generation is defined as:

$$S_h = \frac{\lambda}{T_b^2}\left[\left(\frac{\partial T}{\partial x}\right)^2 + \left(\frac{\partial T}{\partial y}\right)^2 + \left(\frac{\partial T}{\partial z}\right)^2\right] \tag{5}$$

The viscous dissipation entropy generation is expressed as:

$$S_d = \frac{\mu}{T_b}\left\{\begin{array}{c} 2\left[\left(\frac{\partial u}{\partial x}\right)^2 + \left(\frac{\partial v}{\partial y}\right)^2 + \left(\frac{\partial w}{\partial z}\right)^2\right] + \left(\frac{\partial u}{\partial y} + \frac{\partial v}{\partial x}\right)^2 + \left(\frac{\partial u}{\partial z} + \frac{\partial w}{\partial x}\right)^2 \\ + \left(\frac{\partial v}{\partial z} + \frac{\partial w}{\partial y}\right)^2 \end{array}\right\} \tag{6}$$

where Tb is the bulk fluid temperature, λ is thermal conductivity, μ is dynamic viscosity, and u, v, w are velocity components. The straight channel shows high S_h due to weak turbulence and thick thermal boundary layer. The reflux channel has high S_d due to strong flow separation and friction loss. The

zigzag channel obtains the lowest S_{total}, indicating the best energy efficiency.

3.5 Heat-Transfer Performance of the Zigzag Flow Channel

The temperature and flow - rate changes at the cold - and hot - fluid inlets are selected as the operable variables. These changes are used to study their effects on heat - transfer performance. The heat - transfer coefficient and Nusselt number obtained in the simulation are important parameters affecting heat -transfer performance. The Nusselt number is calculated as follows:

$$Nu = \frac{hL}{K} \tag{7}$$

where L denotes length and K thermal conductivity, the theorem posits that any physically consistent equation can be expressed as a zero function of dimensionless numbers[34]. Key dimensionless parameters in this study include Nusselt (Nu), Reynolds (Re), and Prandtl (Pr) numbers. These parameters simplify complex heat transfer and flow relationships into universal mathematical expressions, enabling unified analysis across different conditions and scales. This facilitates cross-scale law extraction and engineering applications.

As shown in Figure 12, cold and hot inlet temperatures were varied separately, with Nu_1 and Nu_2 denoting the cold and hot fluid Nusselt numbers, respectively. Fig. 12(a) shows that adjusting the cold inlet temperature leaves both Nu_1 and Nu_2 nearly unchanged. Fig. 12(b) indicates that varying the hot inlet temperature slightly increases Nu_2 (enhancing heat transfer) while Nu_1 remains stable.

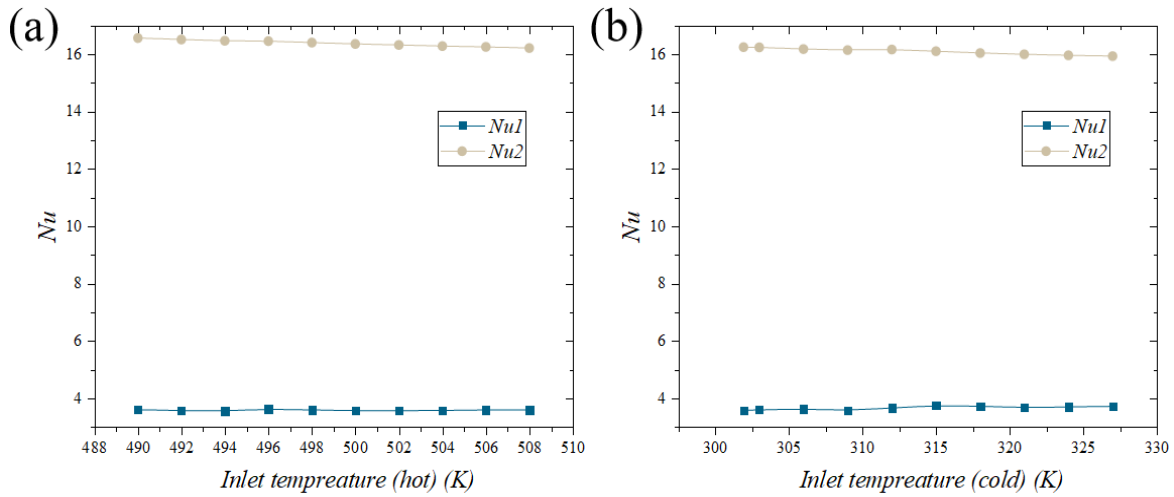

Figure 12. Heat - Transfer Performance with Temperature Changes: (a) Cold Inlet; (b) Hot Inlet

In addition to changing the temperature, changing the flow rate is also crucial for heat - transfer performance. As shown in Figure 13, when the flow rates of the cold and hot fluids are kept the same, it is observed that the Nusselt number increases with the increase in flow rate, and the heat -transfer coefficient also rises with the increase in flow rate. This is because the increase in flow rate enhances convective heat transfer, thereby affecting the increase in the Nusselt number. When the flow rate increases from 0.0016 kg/s to 0.0028 kg/s, the heat -transfer coefficient of the cold fluid increases by approximately 40% to 50%. The increase in the heat -transfer coefficient of the hot fluid is about 50% to 55%, indicating that the flow rate has a significant impact on heat -transfer efficiency. Appropriately

increasing the flow rate helps to improve heat -transfer efficiency.

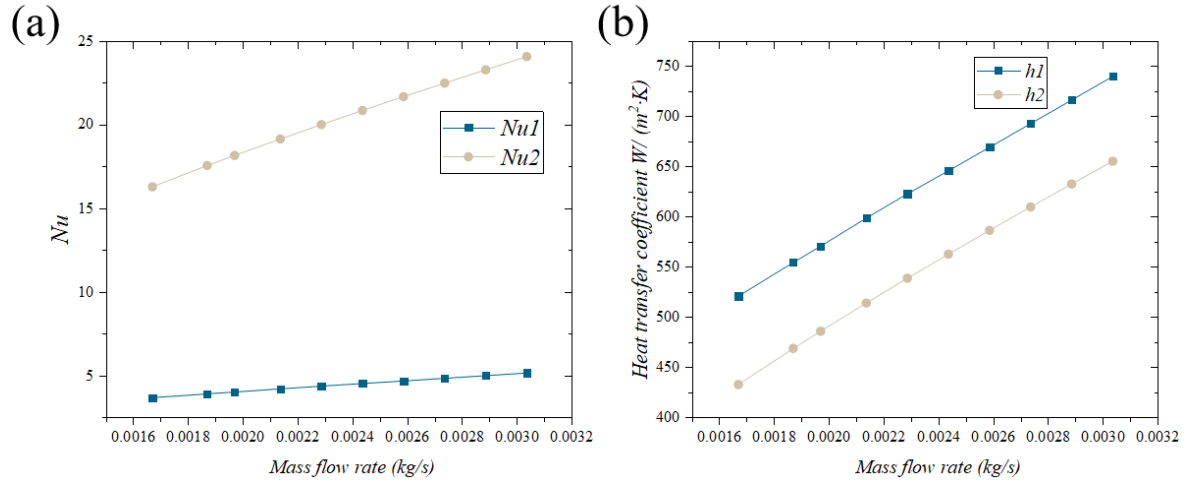

Figure 13. Heat - Transfer Performance with Flow - Rate Changes: (a) Nusselt Number; (b) Heat - Transfer Coefficient

4. Derivation and Verification of Heat - Transfer Correlations

4.1. Derivation of Heat - Transfer Correlations

This study integrated experimental and simulation data, using genetic algorithms to model the heat-transfer characteristics of a system's hot and cold ends. It derived high-precision heat-transfer correlations, with the algorithm searching for optimal solutions in multidimensional data space via biological evolution-inspired mechanisms. Using data from diverse working conditions, the study constructed a robust model capturing the link between heat-transfer coefficients and influencing factors, providing new insights for heat-transfer system design and optimization.

The correlation equation for the hot side:

$$Nu = 2.09Re^{0.279}Pr^{0.3} \tag{8}$$

This correlation uses Nu (Nusselt number), Re (Reynolds number), and Pr (Prandtl number) for the hot side. Derived from simulation data analysis, it captures the hot-side fluid's heat transfer under diverse flow conditions and thermophysical properties. Re reflects flow turbulence (higher Re = stronger turbulence = better heat transfer), while Pr shows how fluid thermophysical properties affect heat transfer.

The correlation equation for the cold side：

$$Nu = 0.688Re^{0.139}Pr^{0.3} \tag{9}$$

The cold-side heat transfer is characterized by Nu, Re, and Pr. Due to differences in fluid dynamics and thermophysical properties between the cold and hot sides, the coefficients and exponents in the correlation equation need to be independently calibrated for the cold side. Re governs flow turbulence, while Pr reflects the ratio of momentum to heat transfer. A genetic algorithm was selected as the modeling tool for its strong global optimization capability and ability to handle nonlinear relationships, though it is more computationally intensive and requires more complex parameter configuration than gradient descent.

4.2. Verification of the Accuracy of the Correlation Equations for the Cold and Hot Sides

Multiple simulations verified the accuracy of the derived heat transfer correlation. Fig. 14(a) and (b) compare predicted values with simulation results, with errors controlled within 20% (red lines). The hot-side Nusselt number relative error is 15%, and the cold-side error is generally below 18%, enabling accurate prediction of cyclopentane heat transfer performance in PCHEs. Statistical analysis shows hot fluid Nu_1 ranges from 11.93 to 22.89, and cold fluid Nu_2 ranges from 1.80 to 3.20. The correlation applies to cyclopentane at 150 kPa (mass flow 0.0036-0.1215 kg/s, cooling capacity 8.88-22.68kW) and 1000kPa (mass flow 0.0036–0.1215 kg/s, heating capacity 8.88–22.68 kW), providing a solid theoretical basis for heat exchanger design and performance prediction. It should be emphasized that all correlations and conclusions obtained in this study are only valid within the range of operating conditions and geometric parameters tested in the present work. Extrapolation or application beyond the tested ranges of flow rate, temperature, pressure, and channel size is not recommended, as the prediction accuracy and reliability cannot be guaranteed under untested conditions.

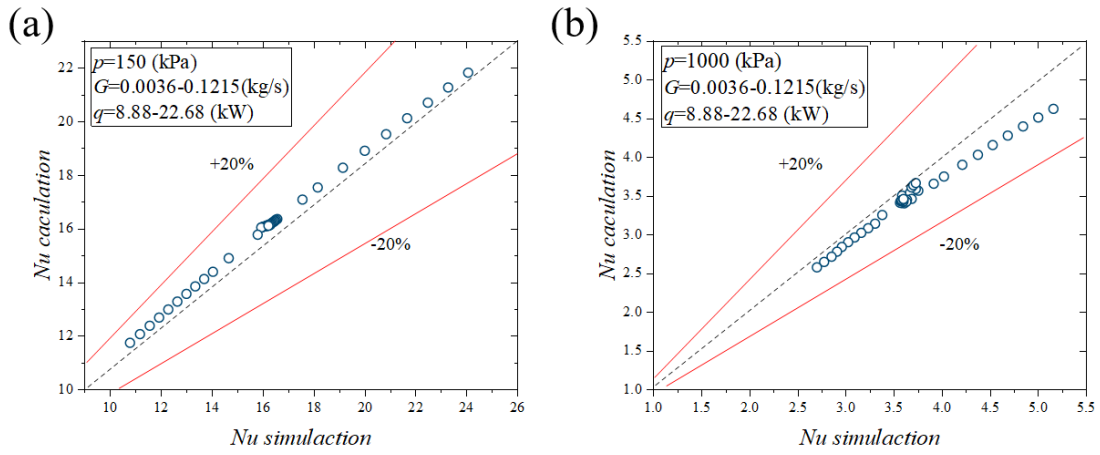

Figure 14. Comparison of Correlation Results with Simulation Results: (a) Hot Fluid; (b) Cold Fluid

Conclusions

This study, based on the heat transfer performance of cyclopentane in a straight flow channel, further proposes reflux and serpentine flow channels. Through comprehensive analysis of these types of flow channels using Fluent computational fluid dynamics simulation, the following conclusions are drawn:

1. Flow Channel Structure Optimization and Performance Comparison: Three types of flow channel models, namely straight, reflux, and serpentine, were constructed to analyze the heat transfer and flow characteristics of cyclopentane. Under the same core volume and boundary conditions. The straight channel has the shortest flow path and weakest turbulence, showing the lowest heat transfer rate. The serpentine flow channel enhances fluid disturbance through its zigzag path, reducing the pressure drop on the cold and hot sides by 60.61% and 87.88%, respectively, compared to the reflux flow channel. Meanwhile, the heat transfer rate is increased by 198.75% compared to the straight flow channel.

2. Construction and Validation of Heat Transfer Correlations: Based on genetic algorithm,

experimental and simulation data under conditions of 150 kPa and 1000 kPa were integrated to derive heat transfer correlations applicable to cyclopentane PCHE. The prediction errors of the correlations for both the hot and cold sides are controlled within 20% compared to the measured values, effectively capturing the heat transfer characteristics of cyclopentane in microchannels.

3. Engineering Application Value and Theoretical Contribution: The serpentine flow channel design can increase the heat transfer per unit volume of PCHE in ORC systems by approximately two times and reduce the pumping energy consumption by over 30%.

Acknowledgment: The Key Natural Science Project of Anhui Provincial Department of Education (No.2024AH051513); Talent Research Fund of Hefei University (24RC01).

References

[1] Bai, T., *et al.*, Thermodynamic analysis of exhaust waste heat recovery in a compound open absorption heat pump system, *Applied Thermal Engineering*, *257* (2024), DOI No. 10.1016/j.applthermaleng.2024.124387

[2] Narwal, K., *et al.*, Enhanced energy storage density in thermal energy storage systems simultaneously heated with solar radiation and industrial waste heat, *Results in Engineering*, *25* (2025), DOI No. 10.1016/j.rineng.2024.103792

[3] Du, K., *et al.*, A state-of-the-art review of the application of phase change materials (PCM) in Mobilized-Thermal Energy Storage (M-TES) for recovering low-temperature industrial waste heat (IWH) for distributed heat supply, *Renewable Energy*, *168* (2021), pp. 1040-1057, DOI No. 10.1016/j.renene.2020.12.057

[4] Wiśniewska, P., *et al.*, Waste tire rubber devulcanization technologies: State-of-the-art, limitations and future perspectives, *Waste Management*, *150* (2022), pp. 174-184, DOI No. 10.1016/j.wasman.2022.07.002

[5] Chen, T., *et al.*, Performance evaluation of metal-foam baffle exhaust heat exchanger for waste heat recovery, *Applied Energy*, *266* (2020), DOI No. 10.1016/j.apenergy.2020.114875

[6] Su, B., Research and application of thermal energy recovery and automatic monitoring system for motor equipment, *Thermal Science*, *28* (2024), 2 Part B, pp. 1397-1404, DOI No. 10.2298/tsci2402397s

[7] Radulovic, J., Organic Rankine cycle: effective applications and technological advances, *Energies*, *16* (2023), 5, DOI No. 10.3390/en16052329

[8] Liu, H., *et al.*, Experimental investigation of a splitting organic Rankine cycle for dual waste heat recovery, *Energy Conversion and Management*, *320* (2024), DOI No. 10.1016/j.enconman.2024.119005

[9] Dong, X., *et al.*, Optimizing waste heat recovery with organic Rankine cycles: A novel graphical approach based on Exergy-Enthalpy diagrams, *Energy*, *311* (2024), DOI No. 10.1016/j.energy.2024.133279

[10] Xia, J., *et al.*, Performance assessment and multi-objective optimization of a novel transcritical CO2 Rankine cycle for engine waste heat recovery, *Case Studies in Thermal Engineering*, *62* (2024), DOI No. 10.1016/j.csite.2024.105223

[11] Klamrassamee, T., *et al.*, Thermodynamic, economic, and carbon emission evaluation of

various Organic Rankine cycle configurations for maximizing waste heat recovery potential, *Energy Conversion and Management: X*, *26* (2025), DOI No. 10.1016/j.ecmx.2025.100943
[12] Wu, X., *et al.*, Efficient predictive control method for ORC waste heat recovery system based on recurrent neural network, *Applied Thermal Engineering*, *257* (2024), DOI No. 10.1016/j.applthermaleng.2024.124352
[13] Zhou, X., *et al.*, Comparative study for waste heat recovery in immersion cooling data centers with district heating and organic Rankine cycle (ORC), *Applied Thermal Engineering*, *242* (2024), DOI No. 10.1016/j.applthermaleng.2024.122479
[14] Bellos, E., *et al.*, Thermodynamic investigation of a novel organic Rankine cycle including partial evaporation, dual-phase expander, flash tank, dry expander and recuperator for waste heat recovery, *Thermal Science and Engineering Progress*, *46* (2023), DOI No. 10.1016/j.tsep.2023.102244
[15] Kittijungjit, T., *et al.*, Comprehensive study on waste heat recovery from gas turbine exhaust using combined steam Rankine and organic Rankine cycles, *Energy Conversion and Management: X*, *25* (2025), DOI No. 10.1016/j.ecmx.2024.100825
[16] Mohammad Bahrami, F.P.,A.K. , Low global warming potential (GWP) working fluids (WFs) for Organic Rankine Cycle (ORC) applications, *Energy, 8* (2022), DOI No. 10.1016/j.egyr.2022.01.222
[17] Li, Z., *et al.*, Evaluation and development of Nusselt number and friction factor correlations for airfoil-fin printed circuit heat exchangers, *International Journal of Heat and Mass Transfer*, *253* (2025), DOI No. 10.1016/j.ijheatmasstransfer.2025.127512
[18] Liang, Z., *et al.*, Thermodynamic performance of organic rankine cycle based pumped thermal energy storage system with different working fluids, *Heliyon*, *11* (2025), 1, DOI No. 10.1016/j.heliyon.2024.e41052
[19] Baigh, T. A., *et al.*, Enhancing thermodynamic performance with an advanced combined power and refrigeration cycle with dual LNG cold energy utilization, *Heliyon*, *10* (2024), 15, DOI No. 10.1016/j.heliyon.2024.e35748
[20] Fatigati, F., *et al.*, Model-based assessment of a feedforward-feedback control strategy for ORC-based unit in waste heat recovery application, *Applied Thermal Engineering*, *258* (2025), DOI No. 10.1016/j.applthermaleng.2024.124774
[21] Lee, S. W., *et al.*, Condensation heat transfer and applicability assessment of a printed circuit heat exchanger as a condenser in a cryogenic CO2 capture and storage system, *Applied Thermal Engineering*, *261* (2025), DOI No. 10.1016/j.applthermaleng.2024.125133
[22] Chowdhury, A. S., Ehsan, M. M., A critical overview of working fluids in organic Rankine, supercritical Rankine, and supercritical Brayton cycles under various heat grade sources, *International Journal of Thermofluids*, *20* (2023), DOI No. 10.1016/j.ijft.2023.100426
[23] Chai, L., Tassou, S. A., Influence of operation parameters on thermohydraulic performance of supercritical CO2 in a printed circuit heat exchanger, *Heat Transfer Engineering*, *46* (2024), 16-17, pp. 1457-1475, DOI No. 10.1080/01457632.2024.2384157
[24] Tang, Z., *et al.*, Non-equilibrium overlapping grid method with two-phase porous media model for printed circuit heat exchanger based steam generator, *International Journal of Heat and Mass Transfer*, *232* (2024), DOI No. 10.1016/j.ijheatmasstransfer.2024.125960

[25] Chen, W., *et al.*, Adaptability analysis of flow and heat transfer multi-scale numerical method for printed circuit heat exchanger*, Energy*, *11* (2024), DOI No. 10.1016/j.heliyon.2024.e41052
[26] Yu, G.*, et al.*, Research on the thermal and flow characteristics of novel micro-channel PV/T collectors*, Thermal Science*, *28* (2024), 2 Part C, pp. 1865-1879, DOI No. 10.2298/tsci230522227y
[27] Xinrui, Z.*, et al.*, Numerical investigations of flow and heat transfer characteristics of a regenerative cooling channel using supercritical CO2 with different cross-section shapes*, nternational Journal of Thermal Sciences*, *215* (2025), DOI No. 10.1016/j.ijthermalsci.2025.109965
[28] Kim, I. H., Sun, X., CFD study and PCHE design for secondary heat exchangers with FLiNaK-Helium for SmAHTR*, Nuclear Engineering and Design*, *270* (2014), pp. 325-333, DOI No. 10.1016/j.nucengdes.2014.02.003
[29] Ghoreishi, Z.*, et al.*, The effect of channel dimensions and configuration of thermoelectric elements on the performance of thermoelectric generator module for waste heat recovery*, International Journal of Heat and Mass Transfer*, *203* (2023), DOI No. 10.1016/j.ijheatmasstransfer.2022.123787
[30] Qin, X.*, et al.*, Experimental and simulation-based development of heat-transfer correlations for cyclopentane PCHE*, Energies*, *18* (2025), DOI No. 10.3390/en18112744
[31] Kazaz., O., Abu-Nada, E., Eiyad, Innovative high-energy nanocomposite absorbers for superior solar-driven water desalination through broadband solar energy harvesting, *Applied Thermal Engineering, 273* (2025), DOI No. 10.1016/j.applthermaleng.2025.126531
[32] Sun, J.*, et al.*, Comparative thermodynamic and frictional characteristics of supercritical LNG in a PCHE with teardrop dimples and protrusions under single and coupled rolling-heaving ocean motions*, Ocean Engineering*, *333* (2025), DOI No. 10.1016/j.oceaneng.2025.121484
[33] Sun, J.*, et al.*, Buoyancy effect on entropy generation and heat transfer performances of transcritical liquefied natural gas in a printed circuit heat exchanger*, International Journal of Thermal Sciences*, *212* (2025), DOI No. 10.1016/j.ijthermalsci.2025.109761
[34] Huang, Y., Weibel, J. A., Topology optimization of coral-like heat sinks under pool boiling for two-phase immersion cooling*, International Journal of Heat and Mass Transfer*, *265* (2026), DOI No. 10.1016/j.ijheatmasstransfer.2026.128670

Received: 31.01.2026.
Revised: 24.04.2026.
Accepted: 11.05.2026.